DOI: https://doi.org/10.1016/j.solener.2022.06.010

This is the accept manuscript of the following article that appeared in final form in
Solar Energy 241: 248-261 (2022),
which has been published in final form at
https://doi.org/10.1016/j.solener.2022.06.010.

New insights into Mn_2O_3 based metal oxide granulation technique with enhanced chemical and mechanical stability for thermochemical energy storage in packed bed reactors

Daniel Bielsa[a b *], Mikel Oregui[b] and Pedro L. Arias[b]

[a] *Centre for Cooperative Research on Alternative Energies (CIC energiGUNE), Basque Research and Technology Alliance (BRTA), Albert Einstein 48, 01510, Miñano (Álava), Spain*
[b] *University of the Basque Country (UPV/EHU), calle Alameda Urquijo s/n, 48013 Bilbao, Spain*

Corresponding author at: dbielsa@cicenergigune.com

Abstract

High temperature thermochemical energy storage still requires a significant research effort. Most of the research has been carried out with materials at lab-scale and proper material fabrication techniques need to be developed in order to make feasible the upscaling of the technology. Agglomeration, abrasion or low volumetric energy density are some of the negative consequences observed when trying to pass from the powder state to the material shape and amount required for a thermochemical reactor. In this work, a granulation technique is investigated, using a Si-doped manganese oxide as active material, determining the critical parameters that provide the best chemical and mechanical stability of the granules. The granulation process uses a polymeric binder to give consistency to the granules and afterwards, it is removed to create a porous structure to facilitate the oxygen diffusion in and out of the granule. We identified the importance of decreasing the solubility of the binder to increase the volumetric energy density of the granules. Furthermore, it was observed that increasing the mechanical stability through a high temperature treatment does not decrease the chemical stability of the material. In order to provide the first insights into the scalability of the solution, the chemical and mechanical stability of the granules has been satisfactorily checked during 100 redox cycles, out of which 50 were carried out in a home-made lab-scale packed bed reactor with an inner diameter of 15 mm and another 50 redox cycles in a simultaneous thermal analyzer.

Keywords: Thermochemical energy storage; Doped metal oxides; Redox reaction; Concentrated solar power plant; Sintering inhibition; Packed bed reactor

1. Introduction

High temperature thermochemical energy storage (TcES) is at an early stage of development and thus, little experimental research has been reported at reactor scale. For concentrated solar power (CSP) plants, two existing possibilities have been principally considered. On the one hand, direct use of solar radiation, where the thermochemical material absorbs the solar thermal energy in a receiver, which acts at the same time as a reactor. On the other hand, indirect use, where the thermochemical material is stored in a reactor and the heat exchange is carried out by means of an intermediate heat transfer fluid (Zsembinszki et al., 2018). It has to be noted that the selection of the adequate reactor technology cannot be detached from the CSP configuration, provided that it should be integrated into the operation of the plant. There is still little work concerning the configuration of new CSP generation at high temperature. Nevertheless, one preliminary conclusion is that the TcES cannot simply replace a conventional thermal energy storage system in a CSP such as a commercial molten salt system (Schmidt and Linder, 2017) (Pelay et al., 2019) (Ströhle et al., 2016). Overall, taking into consideration the advantages and disadvantages of the reported technologies, packed bed reactors are the simplest in construction, which makes them an appropriate candidate for a first technology upscaling and integration step in CSP plants. They are easy to build and operate but their main drawbacks are the pressure drop inside the bed, that may induce preferred gas channeling and the limited available contact surface of the reactants, which may compromise the thermal power output (Wokon et al., 2017b). In this regard, the thermochemical material properties, namely, shape, size and structural composition and stability may have a significant impact on the performance of a thermochemical packed bed reactor. Consequently, it may become one of the most important challenges of this technology.

Metal oxides are one of the most studied thermochemical materials for high temperature TcES in CSP plants, since air can be used both as heat transfer fluid and as reactant, simplifying the system integration. Nevertheless, most of the scientific studies that aimed to assess the behaviour of metal oxides use only several mg in the form of micro-sized particle powder at lab-scale(Neises et al., 2012) (Pestalozzi, 2013), whereas the technology upscaling up to a packed bed thermochemical reactor for a real application might require kg or even tons of material. This material amount, in the shape of fine powder, may cause extremely high pressure drop and extra pumping power. In addition, fine powder is more prone to agglomerate, which may contribute to enhance channelling and hinder re-oxidation kinetics (Carrillo et al., 2014). Therefore, studies on technology up-scaling consider different material preparation approaches (e. g. material pelletization or granulation, adding supports), in order to produce particles in the scale of mm or cm, with sufficient mechanical and chemical stability capable of withstanding a great number of thermal cycles.

In the case of a thermochemical packed bed reactor, the particles are subjected to different stresses, namely, chemical, mechanical, and thermal stresses. The volume changes due to both phase transitions and thermal expansion and shrinkage, together with the pressure induced by the weight of the upper particle layers cause particle-wall or particle-particle friction, known as ratcheting. In addition, pore reduction caused by particle sintering may create overpressure during gas release in solid-gas thermochemical materials. As a result,

particles can crack, or their surface can be eroded, leading to a decrease on the void fraction due to reallocation of particles. These negative effects can be significant on the lowest layers, which are subjected to higher weight loads. Taking into account the cycling operation nature of the TES systems and the long life-expectancy required for CSP plants, it can lead to a significant increase of the pressure drop or to the collapse of the container wall. Therefore, the metal oxide particles for a real application, together with fast kinetics, should demonstrate sufficient mechanical strength to ensure reliable stability during the lifetime of these TES systems, which may last several decades.

Particle strength can be increased by designing a proper synthesis route (e. g. sol-gel, spray-drying), applying a pre-treatment (e. g. high temperature sintering) or by adding binders or support materials (e. g. Al_2O_3, TiO_2 or ZrO_2), provided that they do not react with the active material leading to thermochemical deactivation. Another possibility is strengthening the particle surface by encapsulation in a strong porous material or by rapid heating and cooling of the particles. The latter would hinder changes in the core of the granules that might damage the thermochemical material properties.

The addition of support materials in manganese-based oxides has been deeply studied both for CO_2 capture through chemical looping and TcES. The attrition resistance of manganese-iron oxide with the addition of Al_2O_3, $MgAl_2O_4$, CeO_2, ZrO_2 and Y_2O_3–ZrO_2 was investigated by G. Azimi in a fluidized bed reactor (Azimi et al., 2014)(Azimi et al., 2015). The materials were prepared by spray-drying and calcinated up to 1200°C during 4 h. The research showed that the crushing strength does not improve substantially with the addition of these supports, with the exception of ZrO_2, where a slight improvement was observed. Looking at chemical looping applications, M. Abian observed that the addition of TiO_2 may double the crushing strength of manganese-iron oxides, reporting values of 3-5 N compared to the 1-2 N of the undoped samples (Abián et al., 2017).

In regard of TcES research, N. C. Preisner studied the effect on the mechanical strength of manganese-iron oxide by adding 20 wt% of different supporting materials, namely of ZrO_2, CeO_2 and TiO_2 for a moving bed reactor. The material was prepared using a build-up granulation technique at 800°C during 10 h. Pure manganese-iron oxide particles showed a clear tendency to agglomerate and to break into fine particles when subjected to thermal cycling in air. Furthermore, the bed volume was increased by 17 % after 30 cycles in a packed bed reactor containing 21 g of material, meaning that coarsening happened to some extent. Nevertheless, both ZrO_2 and CeO_2 contributed to improve the attrition strength, with a slight particle agglomeration and without coarsening. TiO_2 reacts to form another stable phase and thus, it cannot be considered for TcES (Neumann et al., 2018).

Other interesting approaches involved experiments with extruded metal oxide composites (Pagkoura et al., 2015) and with a support structure, i. e. honeycomb, corderites or foams, coated with the active redox material, through which the fluid can flow (Karagiannakis et al., 2016) (Singh et al., 2017) (Agrafiotis et al., 2015b) (Agrafiotis et al., 2015a) (Agrafiotis et al., 2016). The coated structures presented a better integrity over repetitive redox cycles, although the volumetric energy storage is limited by the capacity of the active material loading, leading to a substantial decrease in the energy storage density.

Concerning lab-scale thermochemical reactor testing, spherical shape particles present lower void fraction and better homogeneity within the reactor bed and thus, it has been one of the most targeted material geometries. Spray drying is a commonly used method to make high-performance, fluidizable particles for chemical looping combustion applications. Ibraheam et al. studied the effect on the redox behaviour and sintering of spray-dried particles of manganese oxide with Al_2O_3, ZrO_2, and Fe_2O_3 (Ibraheam et al., 2019). All the materials showed very poor mass change during redox cycling, since they underwent significant sintering during calcination at 1200°C. Nevertheless, ZrO_2 and Al_2O_3 samples demonstrated enough structural stability under the temperatures tested, although Al_2O_3 addition tends to form a $MnAl_2O_4$ phase, which is stable at the tested temperatures. Wokon et al. studied the kinetic performance of manganese-iron oxide granules of 1-3 mm prepared by a build-up granulation technique without any support or binder in a thermobalance (Wokon et al., 2017a). The corresponding amounts of Mn_3O_4 and Fe_3O_4 powders were mixed in an Eirich mixer, based on the principle of intensive mixing by an inclined arranged rotating mixing pan, providing mixing effect in vertical and horizontal directions through the application of a rotating micro-granulator mixing tool. It was observed a significant particle volume increase after 100 redox cycles, which led to lower density and more fragile particles. This fact might compromise the stability within continuous redox cycling at a real scale and therefore, their mechanical stability shall be enhanced.

Hamidi et al. synthesized granules of manganese-iron oxide by intensive mixing in an Einrich mixer, introducing a maltodextrin solution organic binder at the end of the mixing process (Hamidi et al., 2019). Particle sizes of 0.5 - 1 mm were used to study the reduction reaction of manganese-iron oxide in a small packed bed reactor containing approximately 35 g of the thermochemical material. No data regarding the mechanical properties and stability of the particles under cycling was provided. Another approach was studied by Gigantino et al., who modified a lab-scale granulation process, known as drop technique, to obtain CuO particles of 1-2 mm of diameter (Gigantino et al., 2020). The process consisted in dissolving an organic polymer with the active material to create a paste that is added dropwise to a bath where the immiscibility leads to particle sphericity. Different combinations of polymers, solvents and surfactants were studied, selecting the best combination which led to the highest particle strength and sphericity, even though no data regarding the influence on the reaction kinetics and storage density was reported. In addition, in order to reduce the sintering effect, the CuO powder was mixed with a Y_2O_3/ZrO_2 stabilized powder, turning into less agglomeration after 100 redox cycles, for amounts of Y_2O_3/ZrO_2 above 50 wt%.

Considering that adding a support material decreases the volumetric energy storage density and may deactivate the thermochemical material by undesired chemical reactions, we present a comprehensive study of the granulation technique proposed by Gigantino et al., applied to Si-doped manganese oxide. In a previous work we demonstrated the improved kinetics and chemical stability of Si-doped manganese oxide in powder state, representing a promising material candidate for technology upscaling (Bielsa et al., 2020), which stores and releases heat according to the following equation:

$$6(Mn_{0.99}Si_{0.01})_2O_3(s) + 149\,J/g \leftrightarrow 4(Mn_{0.99}Si_{0.01})_3O_4\,(s) + O_2\,(g) \qquad \text{Eq. 1}$$

The investigation carried out in the present work aims to identify all the effects of the different granulation synthesis parameters on the material behavior, paying special attention to the chemical and mechanical stability and to increase the active material content of the granules, providing new insights into a potential TcES material preparation route for large scale packed bed thermochemical reactors. In the first part of the work, we evaluate the influence of the different synthesis route parameters on the material behavior, from the kinetics to the chemical stability and mechanical behavior of the granules. Subsequently, granules exhibiting the most promising properties were selected for the upscaling study where 8 g of the material was subjected first to 50th redox cycling study in a lab-scale packed bed reactor. Finally, a sample of the tested granules were subjected to additional 50 redox cycles in a STA to analyze in detail their chemical stability after a total of 100 redox cycles. The satisfactory results observed concerning granules mechanical and chemical stability represent a step forward in high temperature thermochemical energy storage upscaling, that can be applicable not only to the material under study but to other metal oxides.

2. Experimental

2.1 Characterization techniques

The particles size and morphology were determined by means of a Quanta 200 FEG scanning electron microscope (SEM) operated in high vacuum mode at 20 kV and with a back scattered electron detector (BSED).

Reaction kinetics and chemical stability were studied with the simultaneous thermal analyzer STA 449 F3 Jupiter (Netzsch). In these studies, samples consisting in 3-4 granules accounting for around 10 mg were placed into 85 µL open platinum/rhodium crucibles (Netzsch) and subjected to charging and discharging cycles under an air stream of 100 mL/min.

The bulk density and true density of the different granules were measured using a helium pycnometer AccuPyc II 1340. For the measurements a reference volume of 1 cm^3 was completely filled with the different composition granules, resulting in total mass varying from 0.1 to 0.3 g.

2.2 Granules synthesis route

The synthesis process applied, based on the methodology developed by Gigantino et al. (Gigantino et al., 2020), consists of the following three steps: i) synthesis step, where the precursors are transformed in a fine powder of the desired material, ii) granulation step,

where spherical granules are produced, and iii) hardening step, consisting in a sintering process to enhance the mechanical stability of the granules.

First, Si-doped manganese oxide samples were synthesized by a sol-gel method, following the procedure described in a previous work (Bielsa et al., 2021). The subsequent granulation technique is based on preparing a mixture of this metal oxide powder and a solution of a polymeric binder and a solvent. Subsequently the mixture is introduced dropwise through a syringe into a precipitating bath, where the drops harden while the solvent leaves the granule. After drying, the granules are calcined to remove the remaining organic matter and to enhance their mechanical stability. As a consequence, the space occupied by the binder becomes empty and then, porous solid granules are obtained. The following two conditions shall be met: the solvent must be miscible with the precipitation bath and the polymeric binder must be soluble in the solvent and insoluble in the precipitation bath. The preparation steps are illustrated in Fig. 1.

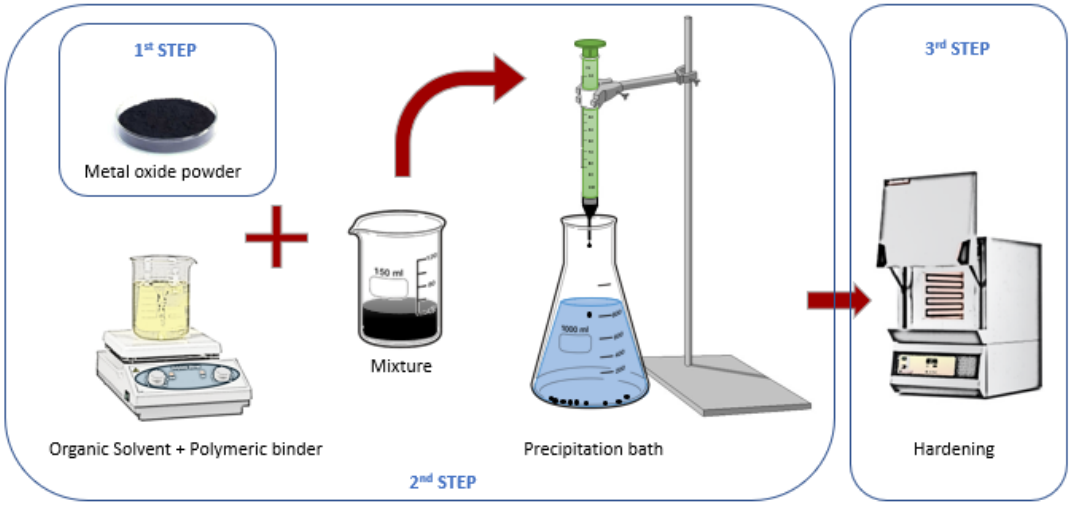

Figure 1. Metal oxide spherical granules preparation route

Various granules of Si-doped Mn_2O_3 were prepared varying the proportions of the metal oxide (MO), organic solvent (OS) and polymeric binder (PB) with the aim of finding the best preparation route giving spherical shape granules with good mechanical and chemical stability. The PB used was ethyl cellulose (Sigma Aldrich) and the OS 1-methyl 2-pyrrolidinone (>99% Sigma Aldrich). The precipitation bath was made of deionized water, mixed with a surfactant (Tween 80, Sigma Aldrich) to reduce its high surface tension and to promote the solvent exit from the granule.

It was found that for the amounts of MO used (< 1 g), the ratio OS:PB shall be maintained in the range 9:1. Lower and higher OS:PB ratio led to inconsistent granules in the precipitation bath and after the hardening step, respectively. In principle, the amount of MO in the granules is important because it might affect directly to the energy storage density, so high proportions are preferred. Nevertheless, high MO proportions (MO/MO+PB > 0.7) increase the viscosity of the mixture resulting in tile-like granules (Fig. 2a), being not practical to increase the MO proportion above 0.8, since the viscosity imposes significant difficulties to the solution to flow

out of the syringe. In order to reduce the viscosity and maintain a high MO content, the OS+PB mixture was heated at 40°C, contributing to improve the sphericity of the granules (Fig. 2b). The distance between the precipitation bath and the syringe tip affected the granules in two ways: distances > 5cm resulted in coin-shape granules due to high mechanical shock when the granules reached the precipitation bath surface, and distances < 2 cm do not allow the granules to penetrate the bath and remain floating in the surface for some time. Therefore, a distance of 3 cm was selected for all the samples. The diameter of the syringe tip has a strong influence on the final size of the granules, which should be maintained below 1:10-20 of the reactor diameter in order to avoid gas channelling inside the thermochemical reactor (Mederos et al., 2009). Therefore, a tip diameter of 2 mm was used, resulting in granules within the average diameter range of 3-4 mm after step 2. Removing the water during the drying step became critical, since it was observed that the water content after the synthesis process may reach up to 80 wt% of the total granule mass and its extraction can destroy the granule sphericity, unless it is carried out slowly. For that reason, the granules were dried at room temperature until the water content was almost totally removed. Subsequently, the granules were subjected to a temperature program consisting in heating up to 450°C at 1°C/min, followed by an isothermal step for 4 h to remove the organic matter (Fig. 2c). The final hardening step consisted in another heating step at 2°C/min up to the corresponding calcination temperature, where different isothermal steps were used to promote particle sintering. A noticeable granule shrinkage was observed during the water and organic matter removal steps, being greater the fewer the content of MO, resulting in granules with a final size of around 1-3 mm of diameter. Table 1 shows the different materials prepared in this work.

a) b) c)

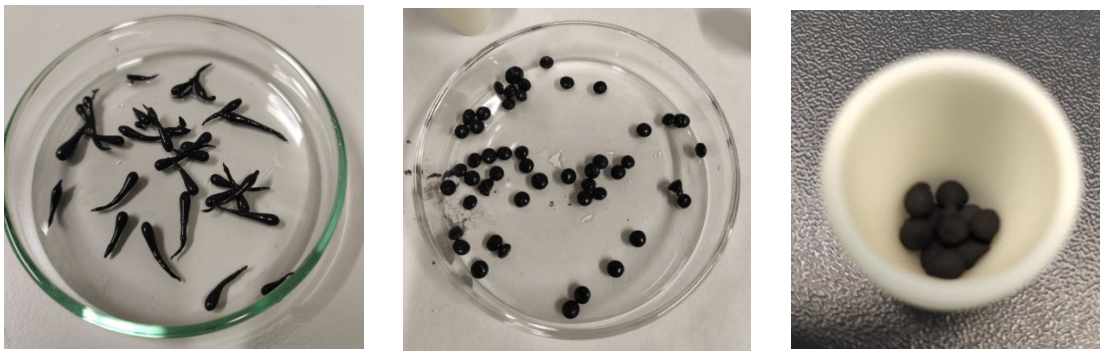

Figure 2. Granules of Mn_2O_3 prepared by the drop technique: a) pronounced tile-like granules, b) spherical granules and c) granules after the calcination step at 450°C

Table 1. Description of materials prepared in this work

Description	MO Proportion (wt %)*	Diameter (mm)
Powder	1	N/A
MO 50	50	1,83
MO 70	70	2,34
MO 80	80	2,46

*MO proportion (wt %) = MO/(MO+PB)

2.3 Experimental setup

The experimental test rig consists of two main parts: the heating setup and the thermochemical reactor (Fig.3a). The generation of a controlled gas flow rate above 800°C required to carry out the reduction and oxidation of the material may become a complex issue and therefore, a furnace placed around the thermochemical reactor carries out the heating/cooling process. The furnace setup temperature was varied between 550°C and 800°C at a heating/cooling rate of 20°C/min and the reactions were conducted switching the gas flow between N_2 and O_2. The thermochemical reactor consists on an AISI 304 metal tube of 15 mm of inner diameter and 400 mm length. Around 8 g of MO were placed in the middle of the tube length. Silicon carbide particles were placed below and above the MO, filling completely the reactor, preventing any movement or fluidization of the MO. Once the gas stream crosses the reactor, it is cooled down in a water bath and subsequently, the oxygen content is measured by means of a zirconia gas analyzer KCD-ON320 (Sensorstecnics). The reactor includes five temperature measuring points at different heights: T2, T3 and T4 placed inside the reactor at the positions indicated in Fig. 3a and $T2_{out}$ and $T4_{out}$ placed on the exterior surface of the reactor at the same height of T2 and T4, respectively. The signals were collected with an acquisition system type ABSD-MD832-81-23-HLP (Yunrunyn) and registered by a homemade Labview app. The complete set-up is illustrated on Fig. 3b.

a) b)

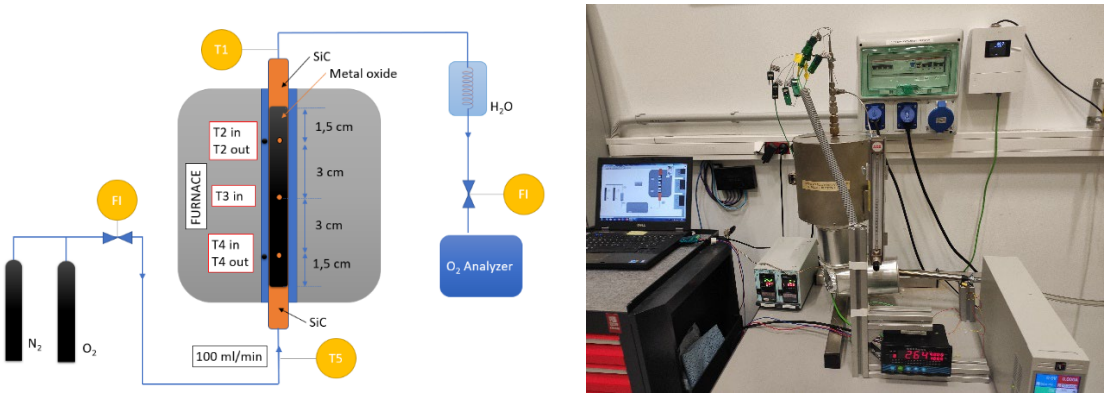

Figure 3. Thermochemical experimental setup: a) components diagram and b) setup photography

3. Results and discussion

3.1 Effects of the synthesis parameters on the granules behaviour

A comprehensive study was made to assess the influence of the granule conformation, the MO content and the hardening step on the chemical and mechanical behavior of Si-doped

Mn_2O_3 granules. In order to identify the influence of the granule conformation on the chemical behavior, the comparison of the mass loss/gain rate between the sample in powder and granule form during one redox cycle is plotted on Fig. 4a. In order to avoid the effects of the hardening step, the granules were subjected to a restricted temperature program up to 450°C for 4 h, aimed to remove the organic matter. As can be inferred from the TGA plot, the reduction reaction kinetics remains similar whereas the oxidation onset temperature is delayed to a lower temperature with a slight slow-down of the reaction kinetics. This effect cannot be attributed to particle sintering during the preparation of the granules since sintering of Mn_2O_3 becomes significant at temperatures above 900°C (Bielsa et al., 2020) and these granules were subjected to significantly lower temperature. Therefore, the results suggest that the particle densification in the granule may have a slight negative impact on the oxygen diffusion rate. This phenomenon, however, does not affect the reversibility of the samples, since after the redox cycle the mass of both samples was equal to their respective initial masses.

Considering that it has been shown that the sintering is the main reason of the cyclability loss in these materials (Carrillo et al., 2014), the hardening program shall be carefully selected to get enough mechanical stability of the granules avoiding critical thermochemical cyclability loss. The resulting granules should have enough mechanical stability to withstand the mechanical stresses occurring in a packed bed reactor while their porous structure should facilitate oxygen diffusion and exchange during system charging and discharging. The influence of the hardening step on the chemical performance of the granules was studied by subjecting the samples to three different temperature programs: 1050°C for 4h, 1050°C for 8h and 1100°C for 4h, and observing their behaviour under 1 redox cycle (Fig. 4b). Again, the reduction reaction did not show any significant variation caused by the hardening step. It should be noted that the granular samples presented a slight decrease on the reduction extent compared to the sample in powder state. This fact can be attributed to an incomplete Si-doping during the synthesis process of the powder, which is further developed during the hardening step of the granules, leading to the formation of more inactive Mn-Si-O bonds and thus, reaching a more chemically stable structure. The same effect was observed in a previous work (Bielsa et al., 2020). On the other hand, the harsh temperature conditions applied caused an additional slow-down on the oxidation reaction kinetics, more pronounced at the second half of the reaction, which will be further analyzed in the cyclability studies. Nevertheless, similar mass gain profiles were observed independently of the hardening program used. This fact may suppose an important advantage since increasing the temperature or the time exposure does not affect negatively the chemical performance, whereas it is expected to significantly improve the mechanical stability.

a) b)

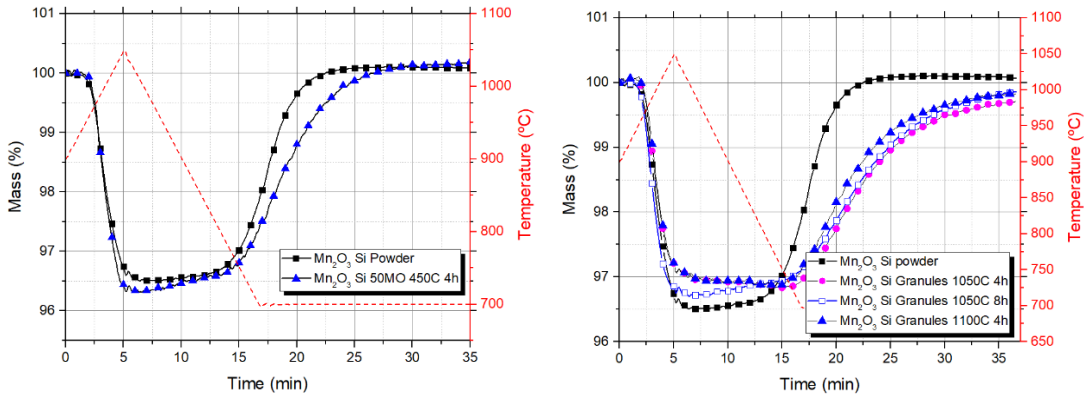

Figure 4. TGA plot of 1 redox cycle to: a) Mn_2O_3-Si powder and Mn_2O_3-Si granules calcined at 450°C 4h and b) Mn_2O_3-Si powder and Mn_2O_3-Si granules calcined at 1050°C 4h, 1050°C 8h and 1100°C 4h.

The effect on the chemical behavior of the MO content in the granules was studied over three samples with the following MO:PB ratios: 50:50, 70:30 and 80:20, calcined at 1050°C for 4h. The three samples together with the sample in powder state were subjected to one redox cycle and the TGA results were overlapped and plotted in Fig. 5a. As can be observed, the reduction reaction kinetics for the three granular samples remains is comparable to the the powder sample. However, the oxidation reaction kinetics exhibits remarkable differences. The higher the MO content the faster the oxidation kinetics, with the sample containing 80% of MO exhibiting a similar performance to the powder sample. It would be expected that the granules with the lowest MO content and consequently, the highest PB content, would present higher voids after PB removal and thus, the oxygen diffusion would encounter less obstacles leading to a faster kinetics. Nevertheless, the removal of water, OS and PB led to a significant decrease of the granule size, as can be observed in Fig.5b and consequently, of the porous volume. This reduction in volume was greater with the decrease of MO content, leading to lower pore volume, which would hinder the oxygen diffusion into the particles.

a) b)

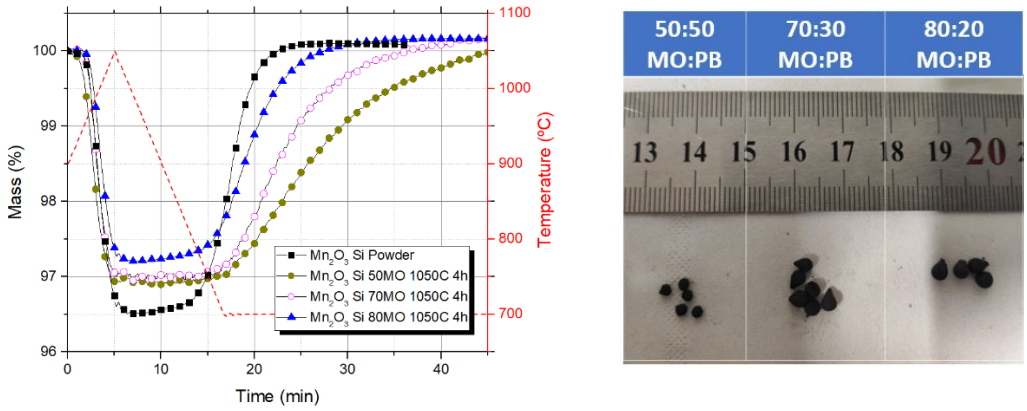

Figure 5. a) TGA plot of 1 redox cycle to Mn_2O_3-Si powder and Mn_2O_3-Si granules calcined at 1050°C 4h with different MO:PO proportions (80:20, 70:30 and 50:50) and b) Mn_2O_3-Si granules picture with different MO:PO proportions (80:20, 70:30 and 50:50)

In a previous work, Mn_2O_3 1% Si-doped material showed good chemical stability over 40 redox cycles in the form of powder. Nevertheless, taking into consideration the results observed in

the TGA measurements, the influence of both the particle densification in the granules and the hardening step will be evaluated prior to upscale the solution to the thermochemical lab-scale reactor. For this purpose three batches of granules were prepared with a MO content ratio 70:30 (MO:PB) and calcined at 1050°C for 4h, 1050°C for 8h and 1100°C for 4h. The chemical stability of the three samples together with the sample in the form of powder were studied over 10 redox cycles in a thermobalance. In this case, Mn_2O_3 Si-doped sample in the form of powder showed a significant reversibility improvement compared to that of pure Mn_2O_3 sample (Fig. 6a and 6b), similar behavior was observed in a previous work, where Si acted as a sintering inhibitor and oxidation accelerator (Bielsa et al., 2020). The three granular samples showed complete reversibility over 10 redox cycles (Fig. 6c, 6d and 6f), meaning that neither the granule shape nor the hardening program have a significant negative impact on the reversibility of the material, as was the case of Mn_2O_3 pure samples. In this case, the positive effects of doping Mn_2O_3 with Si, counteracted the barriers imposed by the granulation and the hardening program to the oxygen diffusion inside the material, improving the material chemical stability. This effect is confirmed if the oxidation reaction kinetics is analyzed in detail throughout the 10 redox cycles, where it can be observed that applying any of the hardening programs led to a negligible slowdown of the oxidation reaction kinetics no matter what calcination temperature or isothermal exposure time were used (Fig. 7). The dependence between the temperature program and the oxidation rate decay on manganese oxide was observed by A. J. Carrillo et al., where using 1050°C instead of 1000°C as the maximum temperature of the redox cycles led to a significant sintering of the particle grains and a complete deactivation of the manganese oxide sample studied (Carrillo et al., 2015). Therefore, the observed tolerance of the Si-doped granules to high temperatures may represent a significant advantage to improve the mechanical stability without decreasing the chemical performance.

In order to provide more insights into the chemical stability of the granules, the particle morphology and the sintering effects were studied by SEM. Sintering effects on metal oxides are particle growth and densification. Both have been shown to constitute physical barriers that hinder the oxygen diffusion and thus, the reversibility of the reactions is deteriorated (Wong, 2011). This deterioration is especially significant in the case of the oxidation reaction. Carrillo et al. attributed these negative consequences to the material exposition to the high temperatures required to carry out the redox reactions, causing an evolution from nano-sized particles to particles of several micrometers just after 30 redox cycles (Carrillo et al., 2014). In the present work, the samples were exposed to a first isothermal high temperature hardening program during the granules preparation route to increase the granules crushing strength, followed by a second variable temperature program during cycling to check their chemical stability, involving reduction and oxidation of the sample. The SEM micrographs after the two thermal processes are presented in Fig. 8. As can be inferred from the SEM images, the particle morphology and particle size seem not to be affected by either the calcination temperature or the isothermal exposure time. This fact can be deduced from the similar TG measurement profiles of the three granular samples during the first redox cycle. Furthermore, the particle size remains stable after 10 redox cycles, which comes to confirm an effective sintering protection by Si-doping process.

Nevertheless, the resulting particle morphology after the redox cycles indicates that the sintering pathways during both temperature programs differ at some extent. Particle morphology after the hardening program presents a more loose and non-uniform size distribution of coarsened particles, whereas after the cycling program the particle morphology turned into a higher degree of coral-like array interconnected particles of similar size without a noticeable particle growth from the previous step. It has been observed, that after the 10th redox cycle, the three samples presented a slight oxidation rate decay. This suggests that the woven net formed during the coral sintering pathway hinders the oxygen diffusion into the inner particles, causing a slight slow-down of the oxidation rate. It was shown that the material in the form of powder calcined at 800°C did not present neither this particle morphology evolution nor the oxidation rate decay over a 40 redox cycle program (Bielsa et al., 2020), which may significate that the particle morphology changes induced by the hardening program might weaken the sintering protection given by the Si-doping process. It is worth noting that the operating conditions imposed by the TGA laboratory instrument used can differ from the ones expected in a real packed bed reactor, being considerably less severe for the material. In order to get a complete reduction of the material in the TGA it was required to reach a maximum temperature more than 100°C above the reduction onset temperature of the material. This fact was already observed in a previous work, where isothermal programs did not get further material reduction once the isothermal temperature was reached (Bielsa et al., 2019). The authors attributed to a deficient oxygen gas removal from the particles, caused by the specific configuration of the experiment, where the material is placed in a cylindrical crucible with just one open face. This arrangement may cause an oxygen partial pressure increase and consequently, as the distance to equilibrium decreases with increasing gas partial pressure, it requires a continuous temperature increase to keep reducing the material. A similar behavior was reported by Hamidi (Hamidi et al., 2019), Varsano (Varsano et al., 2016) and Schoenfelder and Swisher (Schoenfelder and Swisher, 1973). Furthermore, the difficulties observed regarding the oxygen diffusion within the particles in the TGA instrument, of critical importance to carry out the oxidation reaction, should present evident improvements in a thermochemical reactor where the gas is pumped through the whole sample in a bottom-up flow. Therefore, the assessment of the chemical stability of the material shall be complemented with a study in a packed bed laboratory set-up.

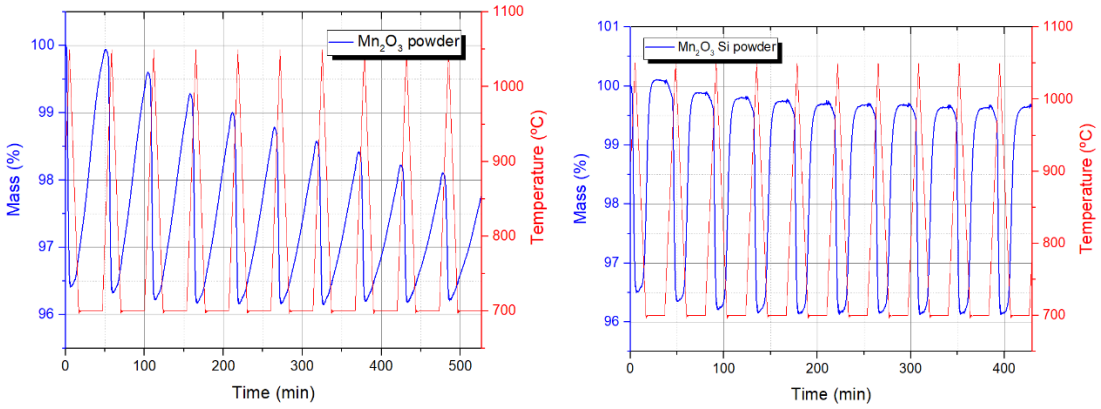

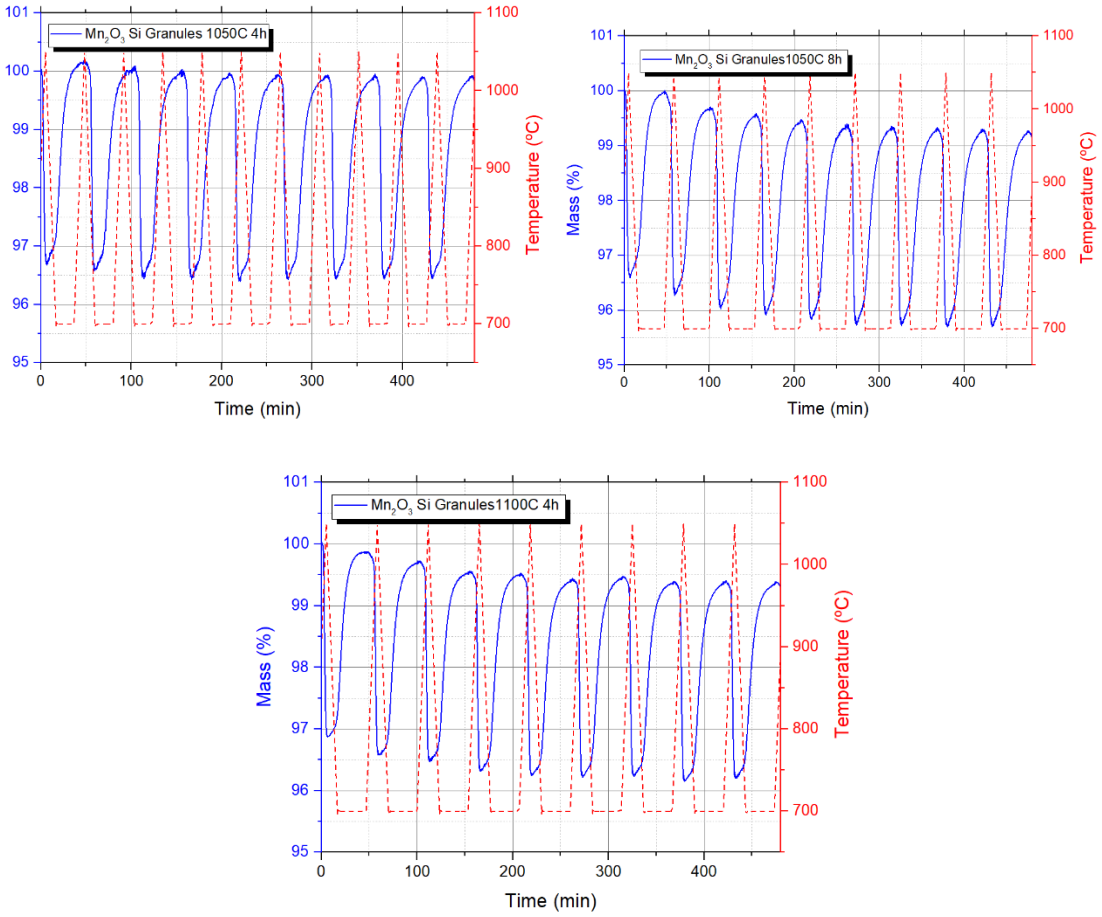

Figure 6. 10 Redox cycles of several Mn_2O_3-Si doped samples sintered at different temperatures: a) Mn_2O_3-Si powder, b) Mn_2O_3-Si granules sintered at 1050°C 4h, c) Mn_2O_3-Si granules sintered at 1050°C 8h, d) Mn_2O_3-Si granules sintered at 1100°C 4h.

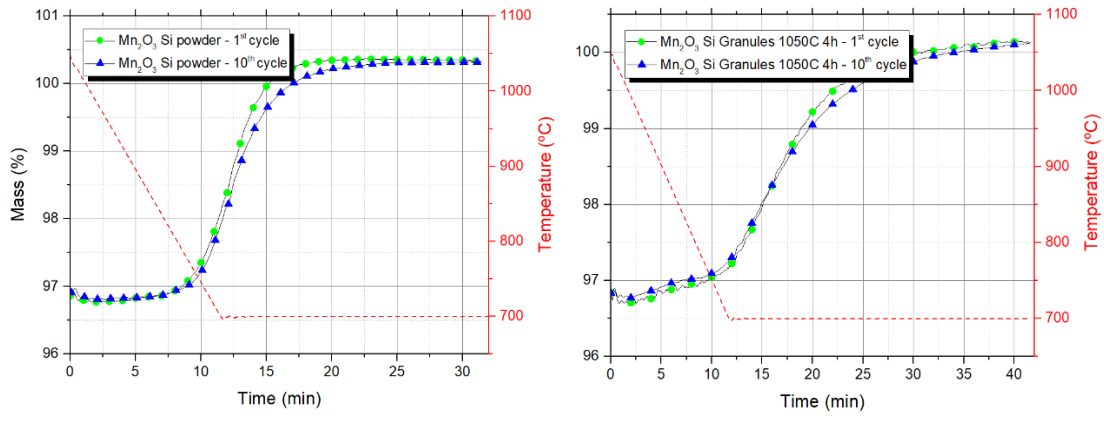

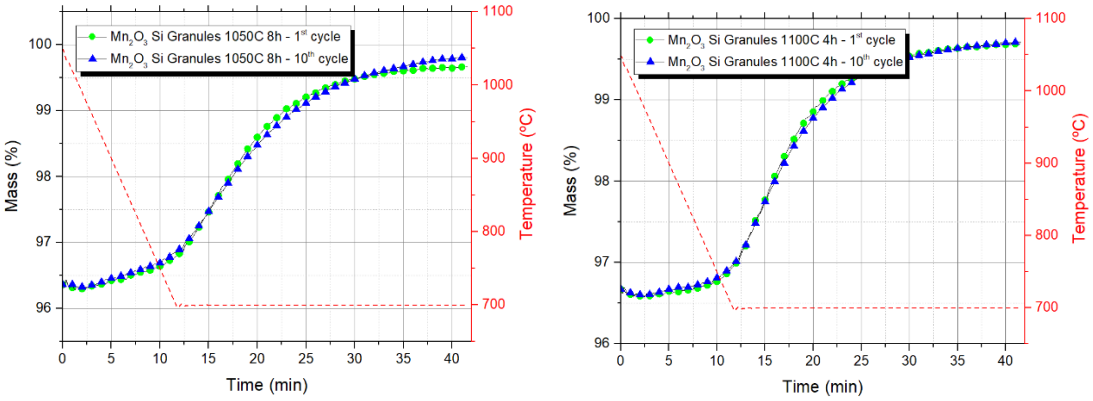

Figure 7. Oxidation reaction TGA plots during the 1st and 10th redox cycle of several Mn_2O_3-Si doped samples sintered at different temperatures: a) Mn_2O_3-Si powder, b) Mn_2O_3-Si granules sintered at 1050°C 4h, c) Mn_2O_3-Si granules sintered at 1050°C 8h, d) Mn_2O_3-Si granules sintered at 1100°C 4h.

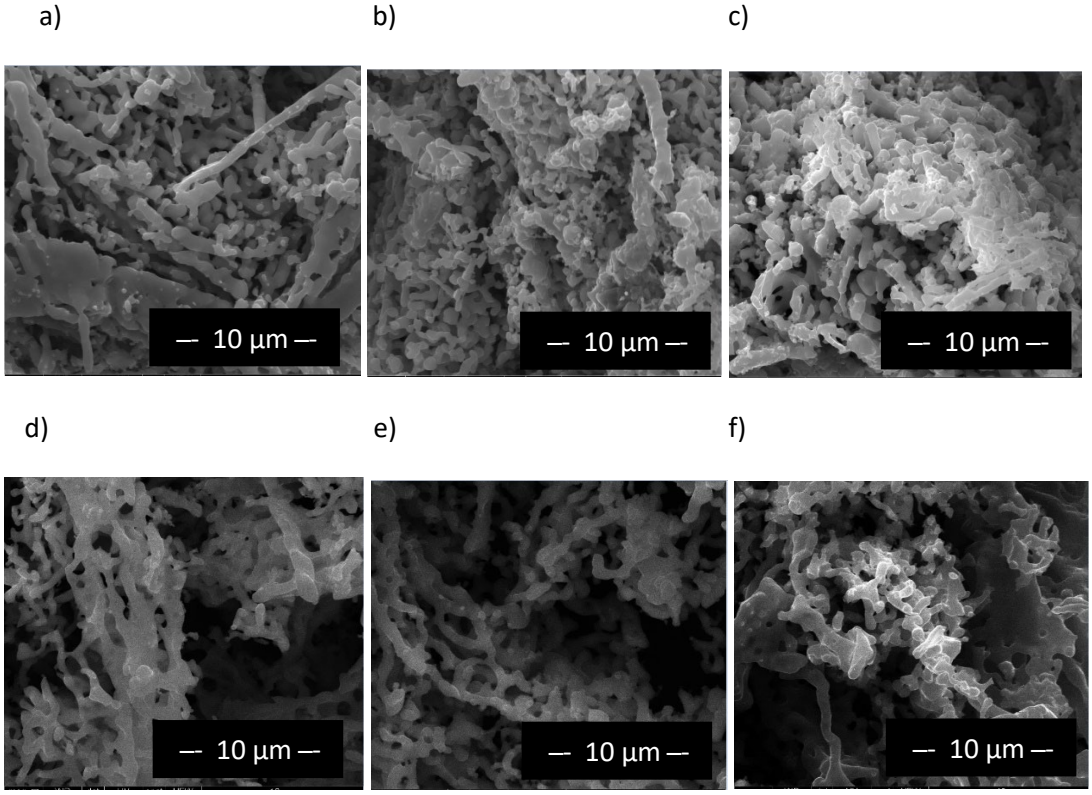

Figure 8. SEM images of the different Mn_2O_3-Si 70MO granules after exposition at different temperature programs: a) 1050°C during 4h, b) 1050°C during 8h, c) 1100°C during 4h, d) 1050°C during 4h and 10 redox cycles, e) 1050°C during 8h and 10 redox cycles and, f) 1100°C during 4h and 10 redox cycles

3.2 Packed bed thermochemical reactor experiments

3.2.1 Granules mechanical stress assessment

In order to assess the mechanical capability of the different calcined granules to withstand the mechanical stresses imposed by the lab-scale packed bed reactor set-up, a layer composed of 3 of the different set of granules was submitted to an increased weight through a flat plate until failure. The crushing strength results are shown in Table 2 and shall be taken only as a reference value for the particular configuration tested in the present work. To obtain an accurate value for the crushing strength specific lab device should be used (e. g. standard compression testing machine).

Table 2. Crushing strength of the granules calcined at different temperature programs

Sample id	Hardening program	Maximum weight	Crushing strength
MO 50	1050°C 4h	38 g	0,126 N
MO 50	1050°C 8h	44 g	0,146 N
MO 50	1100°C 4h	50 g	0,166 N

3.2.2 Selection of the granules for the packed bed reactor experiments

The reactor consisted on a stainless-steel tube of 13 mm of internal diameter and 90 mm height, turning into an effective volume of 11,9 cm^3. In order to determine the energy density contained in this volume it is necessary to measure the actual metal oxide content in the granules and the packed bed void fraction. The metal oxide content in the granules was determined using a reference volume of 1 cm^3. This volume was filled with granules of the different MO:PB ratios used and the bulk density and true density were measured using a helium pycnometer AccuPyc II 1340. It was observed that the maximum MO in the granules reached only 16.94%, likely caused by a deficient dissolution of the OS in the precipitation bath. In order to get an increase on the MO content another batch of granules was prepared decreasing the temperature of the bath by using ice in order to reduce the solubility of the PB (MO 50-c). The resulting granules got a significant MO content increase. The results are showed in Table 3.

Table 3. Samples properties measurement over a reference volume of 1 cm^3

Description	Mass granule g	Diameter mm	Bulk density g/cm^3	True density g/cm^3	MO content %
Powder	N/A	N/A	0,3345	5,3236	N/A
MO 50	0,0023	1,835	0,735	5,116	14,38
MO 70	0,0055	2,342	0,828	5,0047	16,56
MO 80	0,0066	2,466	0,846	5,253	16,94
MO 50-c	0,002	1,396	1,402	5,653	24,81

Considering the size of the lab-scale reactor and the granules with the highest bulk density, the maximum amount of material that can be introduced in the reactor without applying pressure was a maximum of 8 g. Therefore, according to the data provided in Table 2, the three hardening programs provide to the granules with enough mechanical stability to withstand the mechanical stress imposed by the weight of the packed bed. Consequently, the granules with the highest MO content (MO 50-c) calcined at 1050°C for 4h, which in addition

present a more homogeneous sphericity, were selected and synthesized for further cycling tests in the lab-scale reactor (Fig. 9).

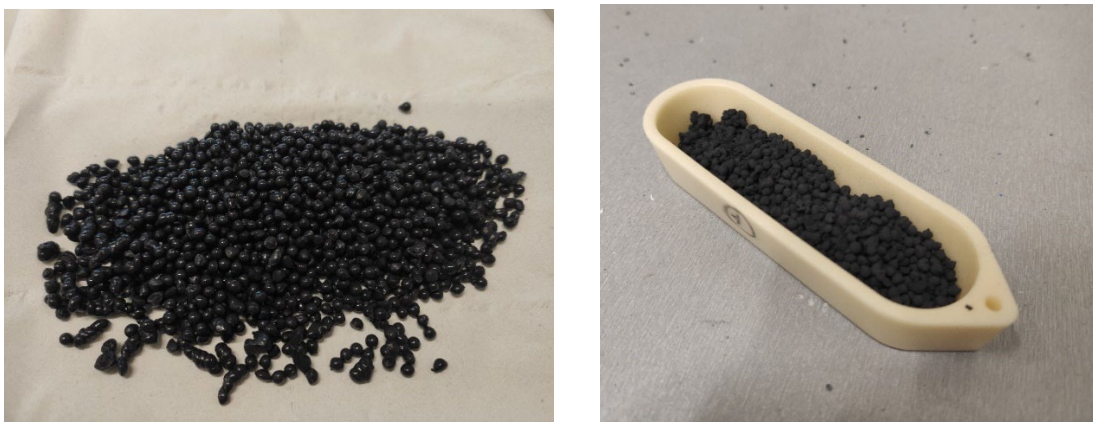

Figure 9. Mn_2O_3 Si-doped granules 50:50 (MO:PB) for reactor testing: a) After step 2 of the synthesis route and b) After hardening at 1050°C for 4 h.

3.2.3 Packed bed reactor experimental results

A summary of the main reactor parameters is presented in Table 4.

Table 4. Lab-scale reactor parameters

Description	Value
Reactor radius	13 mm
Reactor length	90 mm
Particle diameter (d_p)	1,39 mm
Reactor mass	7,96 g
Bulk density	1,402 g/cm^3
Void fraction (ε)	0,59
Material storage density	149 J/g (Bielsa et al., 2021)
Storage capacity	0,33 Wh

In order to evaluate the chemical and mechanical stability of the granules in a packed bed arrangement, the reactor was subjected to 50 redox cycles consisting in of: i) a heating step up to 800°C at 20°C/min under 100 mL/min of N_2, ii) an isothermal step at 800°C for 20 min to ensure complete reduction of the material, since in a previous study, the reduction onset temperature in N_2 was identified at approximately 775°C (Bielsa et al., 2021) , and iii) a cooling step down to 550°C with a cooling rate of 20°C/min under a gas flow of 10%/90% (N_2/O_2). In the same work it was observed that in such conditions, oxidation takes place in less than 5 min, so complete material oxidation is expected during the cooling step, before starting the following redox cycle. The temperature evolution at different points of the reactor and the oxygen content in the gas stream flowing out of the reactor were recorded by the instrumentation during the 50 redox cycles and are plotted in Fig. 10a. For better understanding, the same parameters comprising only the 3rd and 4th cycles are plotted in Fig. 10b.

In regard of the reduction reaction, it is difficult to obtain useful information from the temperature profiles of Fig. 10b, since it seems that reduction takes place when the furnace reaches the temperature set point and reduces the power input, which is followed by an abrupt temperature slowdown that makes it difficult to distinguish the effect of the endothermic reduction reaction in the temperature profiles of the internal thermocouples. The reaction occurrence can be ascertained from the oxygen variation measurement, since an increase of the oxygen content in the gas stream reaching a peak of 5% was detected. Nevertheless, the extent of the reaction cannot be evaluated, since integrating the area under the curve, it results in a value reaching only 6% of the theoretical oxygen release expected, considering a theoretical mass loss of 3%. In the case of the oxidation reaction, the internal recorded temperatures (T2, T3 and T4) present a slightly lower cooling rate than the temperatures recorded outside the reactor ($T2_{out}$ and $T4_{out}$) at the beginning of the cooling step. This fact can be caused by the exothermic nature of the oxidation reaction, even though the starting and finishing point of the reaction cannot be distinguished. Regarding the oxygen concentration, a slight variation during the oxidation reaction can be observed. The exact oxygen decrease cannot be accurately determined as a consequence of the poor sensor resolution. However, both evidences suggests that during the heating step reduction of the material is taking place, while in the cooling step the material is being oxidized.

The morphological evolution and physical integrity of the granules after the 50 redox cycles in the reactor was analyzed both by visual inspection (Fig. 10c) and SEM (Fig. 10d). None of the granules presented the reddish color typical of the reduction phase and thus, showing incomplete oxidation, maintaining their spherical shape after removing them from the reactor. As can be observed from the SEM image, the particles have not suffered from noticeable sintering, since their size remain similar to their initial sate after the hardening step (Fig. 8a). Therefore, no reversibility loss would be expected. To confirm this statement three granules of the already cycled material in the reactor were subjected to an additional 50 redox cycles in the STA, using the same temperature program, completing a total program of 100 redox cycles. The mass loss/gain during the STA program together with a SEM image of the particles after the 100 redox cycles are shown in Fig. 11a and Fig. 11b, confirming no loss of the chemical stability of the granules with no noticeable change on the particle morphology.

a)

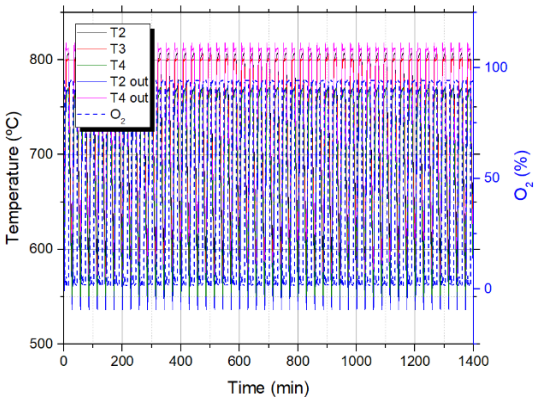

b)

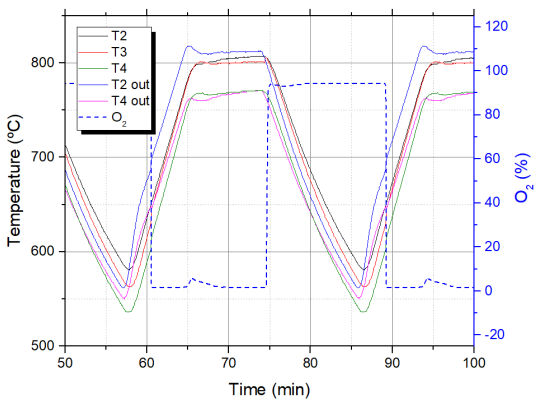

c)

d)

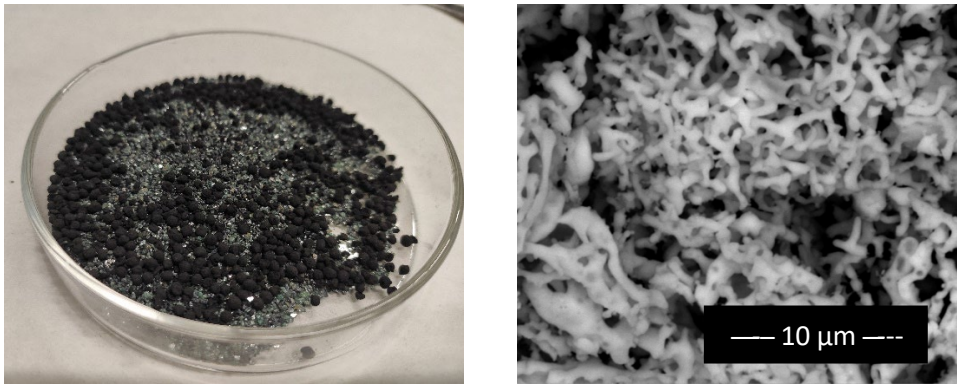

Figure 10. Si-doped Mn_2O_3 granules redox cycling in the thermochemical reactor: a) thermocouples signals record during the whole 50 redox program, b) magnification of the thermocouple signals and oxygen sensor during the 3rd and 4th redox cycle, c) Si-doped granules together with SiC particles appearance after cycling and removing from the reactor, and d) SEM image showing the morphological evolution after the 50th redox cycle

a) b)

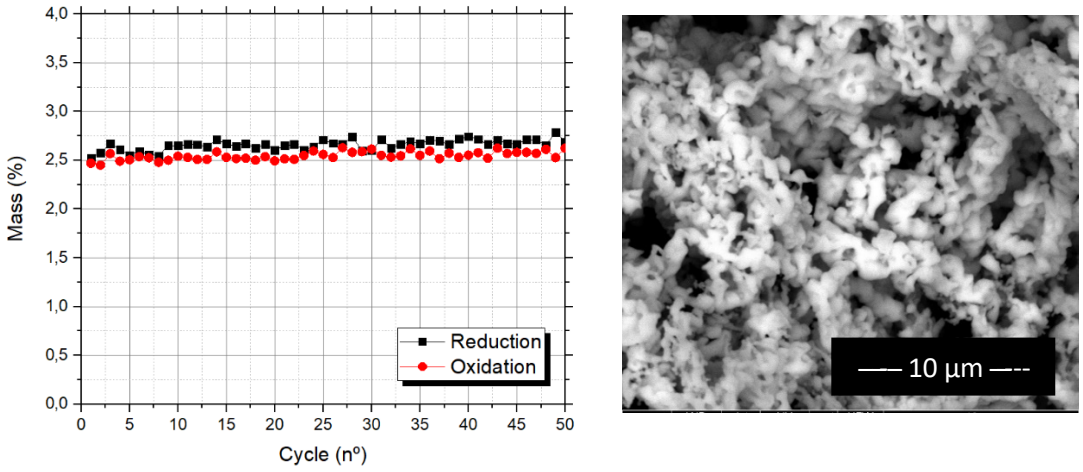

Figure 11. Si-doped Mn_2O_3 granules subjected to 50 additional redox cycles in the STA: a) mass loss/gain recorded in the STA, and b) SEM picture after the additional 50 redox cycles

4. Conclusions

In this work, a granule preparation route was studied for thermochemical energy storage upscaling using a novel Si-doped manganese oxide for concentrated solar power plants. The research work comprises material preparation and thermochemical performance evaluation in a lab-scale packed bed reactor. The process succeeded in obtaining spherical porous granules of 1-2 mm with different active material content. The results identify the critical parameters of the synthesis process which provide the best mechanical and chemical stabilities of the granules in order to be used in a thermochemical packed bed reactor. It was observed that the hardening step aimed to increase the mechanical stability of the granules does not affect significantly their chemical stability. This fact confirms that the severity of the hardening process could be further increased, leading to more mechanically stable granules, required for larger scale reactors. Furthermore, we observed that decreasing the solubility of

the polymeric binder in the synthesis bath almost double the active material content in the granules and consequently, enhances the volumetric energy storage capacity. We achieved an active material content of 24.81%, and this result suggests that there is a way to keep increasing the energy storage density of the granules, which need to be further developed. In addition, 8 g of Si-doped granules were subjected to 50 redox cycles in a lab-scale packed bed reactor, showing satisfactory mechanical and chemical stability, which was confirmed over additional 50 redox cycles in a thermobalance, with complete re-oxidation over the whole program. In summary, both the Si-doped manganese oxide and the granule preparation route conducted have demonstrated enough reliability to be used on a larger scale and thus, contribute to push the high temperature thermochemical storage technology for a next generation of concentrated solar power plants.

Acknowledgements

This work has been supported by the Department of Economic Development and Infrastructures of the Basque government, through the funding of the ELKARTEK CIC Energigune-2017 research program. The authors express their sincere thanks to Cristina Luengo, Mikel Intxaurtieta and Yagmur Polat for their technical support.

Bibliography

Abián, M., Abad Secades, A., Izquierdo Pantoja, M.T., Gayán Sanz, P., Diego Poza, L.F., García Labiano, F., Adánez Elorza, J., 2017. Titanium substituted manganese-ferrite as an oxygen carrier with permanent magnetic properties for chemical looping combustion of solid fuels. Fuel 195, 38–48.

Agrafiotis, C., Becker, A., Roeb, M., Sattler, C., 2016. Exploitation of thermochemical cycles based on solid oxide redox systems for thermochemical storage of solar heat. Part 5: Testing of porous ceramic honeycomb and foam cascades based on cobalt and manganese oxides for hybrid sensible/thermochemical heat storage. Solar Energy 139, 676–694.

Agrafiotis, C., Roeb, M., Sattler, C., 2015a. Hybrid sensible/thermochemical solar energy storage concepts based on porous ceramic structures and redox pair oxides chemistry. Energy Procedia 69, 706–715.

Agrafiotis, C., Roeb, M., Schmuecker, M., Sattler, C., 2015b. Exploitation of thermochemical cycles based on solid oxide redox systems for thermochemical storage of solar heat. Part 2: Redox oxide-coated porous ceramic structures as integrated thermochemical reactors/heat exchangers. Solar Energy 114, 440–458.

Azimi, G., Leion, H., Matisson, T., Rydén, M., Snijkers, F.M.M., Lyngfelt, A., 2014. Mn–Fe Oxides with Support of MgAl2O4, CeO2, ZrO2 and Y2O3–ZrO2 for Chemical-Looping

Combustion and Chemical-Looping with Oxygen Uncoupling. Ind. Eng. Chem. Res 53, 10358–10365.

Azimi, G., Matisson, T., Leion, H., Rydén, M., Lyngfelt, F.M.M., 2015. Comprehensive study of Mn–Fe–Al oxygen-carriers forchemical-looping with oxygen uncoupling (CLOU). International Journal of Greenhouse Gas Control 34, 12–24.

Bielsa, D., Zaki, A., Arias, P.L., Faik, A., 2021. Development of a kinetic reaction model for reduction and oxidation of Si doped Mn2O3 for thermochemical energy storage in concentrated solar power plants. Journal of Energy Storage 43, 103271.

Bielsa, D., Zaki, A., Arias, P.L., Faik, A., 2020. Improving the redox performance of Mn2O3/Mn3O4 pair by Si doping to be used as thermochemical energy storage for concentrated solar power plants. Solar Energy 204, 144–154.

Bielsa, D., Zaki, A., Faik, A., Arias, P.L., 2019. Efficiency improvement of Mn2O3/Mn3O4 redox reaction by means of different operation strategies. https://doi.org/10.1063/1.5117750

Carrillo, A.J., Serrano, D., Pizarro, P., Coronado, J.M., 2014. Thermochemical heat storage based on the Mn2O3/Mn3O4 redox couple: influence of the initial particle size on the morphological evolution and cyclability. J. Mater. Chem. A 2, 19435–19443.

Carrillo, A.J., Serrano, D.P., Pizarro, P., Coronado, J.M., 2015. Improving the Thermochemical Energy Storage Performance of the Mn2O3/Mn3O4 Redox Couple by the Incorporation of Iron. ChemSusChem 8, 1947–1954.

Gigantino, M., Sas Brunser, S., Steinfeld, A., 2020. High-Temperature Thermochemical Heat Storage via the CuO/Cu2O Redox Cycle: From Material Synthesis to Packed-Bed Reactor Engineering and Cyclic Operation. Energy & Fuels 34, 16772–16782.

Hamidi, M., Bayon, A., Wheeler, V.M., Kreider, P., Wallace, M.A., Tsuzuki, T., Catchpole, K., Weimer, A.W., 2019. Reduction kinetics for large spherical 2:1 iron–manganese oxide redox materials for thermochemical energy storage. Chemical Engineering Science 201, 74–81.

Ibraheam, A.S., Ehrhart, B.D., Ward, B.J., Bayon, A., Wallace, M.A., Bader, R., Kreider, P., Weimer, A.W., 2019. Particle design and oxidation kinetics of iron-manganese oxide redox materials for thermochemical energy storage. Solar Energy 183, 17–29.

Karagiannakis, G., Pagkoura, C., Halevas, E., Baltzopoulou, P., Konstandopoulos, A.G., 2016. Cobalt/cobaltous oxide based honeycombs for thermochemical heat storage in future concentrated solar power installations: Multi-cyclic assessment and semi-quantitative heat effects estimations. Solar Energy 133, 394–407.

Mederos, F.S., Ancheyta, J., Chen, J., 2009. Review on criteria to ensure ideal behaviors in trickle-bed reactors. Applied Catalysis A: General 355, 1–19.

Neises, M., Tescari, S., de Oliveira, L., Roeb, M., Sattler, C., Wong, B.Y., 2012. Solar-heated rotary kiln for thermochemical energy storage. Solar Energy 86, 3040–3048.

Neumann, N.C., Block, T., Linder, M., Leion, H., 2018. Stabilizing particles of manganese-iron oxide with additives for thermochemical energy storage. Energy Technology 6.

Pagkoura, C., Karagiannakis, G., Zygogianni, A., Lorentzou, S., Konstandopoulos, A.G., 2015. Cobalt oxide based honeycombs as reactors/heat exchangers for redox Thermochemical Heat Storage in Future CSP Plants. Energy Procedia 69, 978–987.

Pelay, U., Luo, L., Fan, Y., Stitou, D., Castelain, C., 2019. Integration of a thermochemical energy storage system in a Rankine cycle driven by concentrating solar power: Energy and exergy analyses. Energy 167, 498–510.

Pestalozzi, F., 2013. Experimental Investigation of Mn-Based Redox Reaction Kinetics for Thermochemical Energy Storage.

Schmidt, M., Linder, M., 2017. Power generation based on the Ca(OH)2/ CaO thermochemical storage system – Experimental investigation of discharge operation modes in lab scale and corresponding conceptual process design. Applied Energy 203, 594–607.

Schoenfelder, C.W., Swisher, J.H., 1973. Kinetics of Thermal Decomposition of TiH2. Journal of Vacuum Science and Technology 10. https://doi.org/10.1116/1.1318443

Singh, A., Tescari, S., Lantin, G., Agrafiotis, C., Roeb, M., Sattler, C., 2017. Solar thermochemical heat storage via the Co3O4/CoO looping cycle: Storage reactor modelling and experimental validation. Solar Energy 144, 453–465.

Ströhle, S., Haselbacher, A., Jovanovic, Z.R., Steinfeld, A., 2016. The Effect of the Gas-Solid Contacting Pattern in a High-Temperature Thermochemical Energy Storage on the Performance of a Concentrated Solar Power Plant. Energy & Environmental Science 9, 1375–1389.

Varsano, F., Alvani, C., la Barbera, A., Masi, A., Padella, F., 2016. Lithium manganese oxides as high-temperature thermal energy storage system. Thermochimica Acta 640. https://doi.org/10.1016/j.tca.2016.07.018

Wokon, M., Block, T., Nicolai, S., Linder, M., Schmücker, M., 2017a. Thermodynamic and kinetic investigation of a technical grade manganese-iron binary oxide for thermochemical energy storage. Solar Energy 153, 471–485.

Wokon, M., Kohzer, A., Linder, M., 2017b. Investigations on thermochemical energy storage based on technicalgrade manganese-iron oxide in a lab-scale packed bed reactor. Solar Energy 153, 200–214.

Wong, B., 2011. THERMOCHEMICAL HEAT STORAGE FOR CONCENTRATED SOLAR POWER. Golden, CO (United States). https://doi.org/10.2172/1039304

677 Zsembinszki, G., Sole, A., Barreneche, C., Prieto, C., Fernandez, A.I., Cabeza, L.F., 2018.
678 Review of Reactors with Potential Use in Thermochemical Energy Storage in
679 Concentrated Solar Power Plants. Energies 11, 2358.

680